Nondamaging Retinal Laser Therapy: Rationale and Applications to the Macula

Daniel Lavinsky,[1] Jenny Wang,[2,3] Philip Huie,[3,4] Roopa Dalal,[4] Seung Jun Lee,[4,5] Dae Yeong Lee,[4,6] and Daniel Palanker[3,4]

[1]Department of Ophthalmology, Federal University Rio Grande do Sul, Porto Alegre, Brazil
[2]Department of Applied Physics, Stanford University, Stanford, California, United States
[3]Hansen Experimental Physics Laboratory, Stanford University, Stanford, California, United States
[4]Department of Ophthalmology, Stanford University, Stanford, California, United States
[5]Department of Ophthalmology, Kangwon National University, Chuncheon, South Korea
[6]Department of Ophthalmology, Gachon University Gil Medical Center, Incheon, South Korea

Correspondence: Jenny Wang, 452 Lomita Mall, Stanford, CA 94305, USA;
jywang2@stanford.edu.

DL and JW contributed equally to the work presented here and should therefore be regarded as equivalent authors.

PURPOSE. Retinal photocoagulation and nondamaging laser therapy are used for treatment of macular disorders, without understanding of the response mechanism and with no rationale for dosimetry. To establish a proper titration algorithm, we measured the range of tissue response and damage threshold. We then evaluated safety and efficacy of nondamaging retinal therapy (NRT) based on this algorithm for chronic central serous chorioretinopathy (CSCR) and macular telangiectasia (MacTel).

METHODS. Retinal response to laser treatment below damage threshold was assessed in pigmented rabbits by expression of the heat shock protein HSP70 and glial fibrillary acidic protein (GFAP). Energy was adjusted relative to visible titration using the Endpoint Management (EpM) algorithm. In clinical studies, 21 eyes with CSCR and 10 eyes with MacTel were treated at 30% EpM energy with high spot density (0.25-diameter spacing). Visual acuity, retinal and choroidal thickness, and subretinal fluid were monitored for 1 year.

RESULTS. At 25% EpM energy and higher, HSP70 was expressed acutely in RPE, and GFAP upregulation in Müller cells was observed at 1 month. Damage appeared starting at 40% setting. Subretinal fluid resolved completely in 81% and partially in 19% of the CSCR patients, and visual acuity improved by 12 ± 3 letters. Lacunae in the majority of MacTel patients decreased while preserving the retinal thickness, and vision improved by 10 letters.

CONCLUSIONS. Heat shock protein expression in response to hyperthermia helps define the therapeutic window for NRT. Lack of tissue damage enables high-density treatment to boost clinical efficacy, therapy in the fovea, and retreatments to manage chronic diseases.

Keywords: hyperthermia, retina, laser therapy, nondamaging, heat shock protein, macular disorders, macular telangiectasia, central serous chorioretinopathy

Disorders of the macula, the central area of the retina containing structures responsible for high-resolution vision, can lead to vision impairment and blindness, if untreated. Macular disorders include age-related macular degeneration (AMD), the leading cause of untreatable blindness in the world, diabetic macular edema (DME), chronic central serous chorioretinopathy (CSCR), and idiopathic macular telangiectasia (MacTel). While these disorders have different underlying pathophysiology, treatment for each disease is complicated by proximity to the central part of the macula, the fovea, which is vital for high-acuity vision. Laser photocoagulation, either alone or in combination with anti-VEGF pharmacotherapy or steroids, is the standard of care for retinal diseases including proliferative diabetic retinopathy,[1] DME,[2] CSCR,[3] and retinal vein occlusions.[4] However, conventional photocoagulation produces retinal damage, which is unacceptable near the fovea and precludes multiple retreatments, essential for chronic diseases.

Fundamentally, photothermal therapy is based on conversion of absorbed laser light in the retinal pigment epithelium (RPE) and choroid into heat. In photocoagulation, diffusion of heat from the RPE into the retina leads to thermal damage to photoreceptors or, at higher settings, even to the inner retinal cells. While destruction of a significant fraction of photoreceptors, the most metabolically active and numerous cells in the retina, is desirable to reduce metabolic load and thereby decrease secretion of angiogenic factors from ischemic retina in order to limit neovascularization in proliferative diabetic retinopathy, the role of sparse grid photocoagulation in treatment of macular disorders has never been understood.

Several laser techniques have been developed to reduce retinal damage compared to conventional photocoagulation while maintaining therapeutic benefit. One technique, selective RPE therapy (SRT), uses short laser pulses (~1 μs) to confine heating during the pulse to melanosomes within RPE cells.[5,6] A similar technique with 3-ns pulses is called 2RT.[7] With heat confinement and sufficient laser energy, explosive vaporization of melanosomes produces microbubbles that destroy RPE cells[8] without thermal damage to the adjacent retina. Removal of the cell debris, followed by proliferation and migration of the RPE

from adjacent areas,[9] is thought to clear the Bruch's membrane and rejuvenate RPE cells to provide the therapeutic effect.[10]

Another paradigm assumes that thermal stress to the RPE or retinal cells, rather than tissue damage, is responsible for the therapeutic effect of laser treatment in the macula. Trans-pupillary thermotherapy (TTT) has been suggested as an alternative to photocoagulation in cases of subfoveal leaks.[11] In this approach, 810-nm laser was applied with relatively low average power and very long exposures (60 seconds) over a wide spot on the retina (800 μm),[12] producing a large heating zone. However, lack of temperature control or titration in this procedure resulted in frequent occurrences of significant retinal damage.[13] A pulsed version of a similar near-infrared laser with smaller spot size (125 μm) replaced TTT for nondamaging hyperthermia. The so-called subthreshold diode micropulse (SDM) laser[14] or a similar laser at 577-nm wavelength[15] delivers 100- to 300-ms bursts of pulses of 0.1 to 0.3 ms in duration, with the average power set below the clinically detectable tissue damage threshold by adjustment of the pulse duty cycle and peak power. Unlike SRT, the individual micropulses have much (approximately 100 times) lower peak power and much (100 times) longer duration, so that thermal energy is not confined to melanosomes but rather spreads over the whole RPE cell, resulting in cumulative heating by a few degrees[14] rather than microbubble formation. Subthreshold diode micropulse has been shown to be effective in the treatment of CSCR, reducing the subretinal fluid and improving visual acuity, compared to untreated controls.[16] However, lack of a well-defined dosimetry and titration procedure is reflected in the variable results with this technology.[17–19] Moreover, it is not clear whether "micro-pulse" modulation of the laser power provides any benefits compared to continuous wave (CW) laser of the same average power and duration.[14] The key issue with either modality is to properly titrate the laser settings below the damage threshold, but within the range of clinical response in every patient.

We hypothesized that hyperthermia leads to protein denaturation at a rate quantifiable as a temperature-dependent chemical reaction, and that corresponding cellular responses, such as heat shock expression or irreversible damage, are triggered by the reduction in concentration of the critical molecular components. The temperature-dependent reaction rate is described by the Arrhenius equation, which is parameterized by an activation energy and assumes the absence of cellular repair during hyperthermia.[20] The total effect of this process during the laser pulse is described by the integral of the denaturation rate over the duration of hyperthermia. To assess the temperature distribution in tissue during the laser pulse and the corresponding tissue effect, we developed a retinal thermal model.[20]

Different levels of Arrhenius integral were found to correspond to different clinical grades of retinal lesions, with approximately an order of magnitude difference between the distinguishable grades. To relate the highly nonlinear process of retinal photocoagulation to the laser power and duration, we developed an algorithm called Endpoint Management (EpM), which adjusts the laser power and duration such that a 10× increase in Arrhenius integral value corresponds to a 20% increase in the pulse energy (Fig. 1).[21] Arrhenius integral of $\Omega = 1000$ corresponds to a barely visible lesion, detectable right after the exposure (within 3 seconds). We use such a binary definition of the lesion visibility (yes or no) to simplify titration in each subject. Ten times lower Ω corresponds to lesions that become visible much later due to edema that develops over approximately 30 seconds post laser exposure. Arrhenius integral of $\Omega = 1$ corresponds to the damage threshold of RPE. The EpM algorithm maps a clinically relevant range of calculated Arrhenius integral values to linear steps in
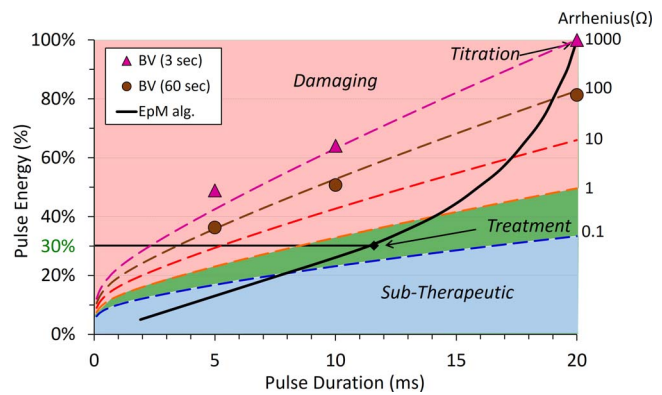

FIGURE 1. Endpoint Management algorithm. *Dashed lines*, corresponding to different clinical grades, differ by an order of magnitude in Arrhenius integral Ω. The *red area* corresponds to the damaging settings and *green* to the nondamaging range of HSP expression; *blue* is below the threshold for cell response. Titration of 100% corresponds to barely visible lesion (BV) observed at 3 seconds.

pulse energy, normalized to a titration dose for producing a barely visible burn at a particular duration (Fig. 1).[21]

Initial experiments with heat shock protein (HSP) expression following retinal exposures in mice indicated that HSP70 is upregulated for $\Omega > 0.1$.[22] Since the damage threshold is $\Omega = 1$, nondamaging thermal therapy corresponds to Arrhenius values in the range of $0.1 < \Omega < 1$.[22] Computational analysis of the clinical laser settings confirmed these estimates.[14]

Within the range of nondamaging hyperthermia, RPE cells respond to thermal stress by expression of HSP.[22] Heat shock proteins are known to act as chaperones for protein refolding, to inhibit apoptosis, and to downregulate inflammation.[23] Induction of these proteins by thermal stress, and activation of the associated downstream repair pathways, is thought to rejuvenate RPE cells and restore their function.[24]

In the retina itself, it has been reported that activation of Müller cells in and around laser lesions (observed by glial fibrillary acidic protein [GFAP] expression) may be responsible for wound contraction and restoration of the photoreceptor layer after thermal damage.[25] Although the exact mechanism of photoreceptor migration into the lesion is not completely understood, it was hypothesized to be mediated by Müller cells, which initially fill the lesion and later contract, thereby pulling in adjacent photoreceptors. This effect could be especially interesting for treating MacTel since it is associated with the focal loss of photoreceptors and is mediated by dysfunction of Müller cells.[26]

Previous studies of the EpM algorithm in rabbits established that, with titration for a barely visible lesion defined as 100% energy on EpM scale, the 30% energy setting corresponds to the RPE damage threshold.[21] In this study, we first define the cellular response window below the damage threshold and the area of RPE activation by imaging the expression of HSP70 in the RPE at various energies and applying live–dead fluorescent assay to map the extent of tissue damage at these settings. Within this window, we also observe the long-term retinal response to nondamaging laser therapy. These preclinical studies helped define the desirable energy range and laser spot density in the treatment pattern. We then applied the EpM protocol with these settings to test the clinical efficacy of nondamaging retinal laser therapy (NRT) in treatment of chronic CSCR and MacTel. In this article, we describe the 1-year results of these studies.

Methods

Laser Treatments in Rabbits

A total of 15 Dutch-belted rabbits were used in accordance with the ARVO Statement for the Use of Animals in Ophthalmic and Vision Research, with approval from the Stanford University Animal Institutional Review Board. The rabbits were anesthetized with ketamine hydrochloride (35 mg/kg) and xylazine (5 mg/kg). Pupil dilation was achieved by one drop each of 1% tropicamide and 2.5% phenylephrine hydrochloride. Topical tetracaine hydrochloride (0.5%) was used for local anesthesia. A Mainster wide-field retinal contact lens (OMRA-WF; Ocular Instruments, Bellevue, WA, USA) was used with hydroxypropyl methylcellulose as a contact gel. The conversion of aerial to retinal beam size with the contact lens on the rabbit eye was calculated to be 70% by comparing pattern spacing on viability-stained samples to aerial pattern spacing.

A 577-nm PASCAL Streamline laser (Topcon Medical Laser Systems, Santa Clara, CA, USA) was used to deliver uniform spots with 200-μm aerial diameter (140-μm on retina). Endpoint Management titration was performed with 20-ms pulses and visibility was evaluated 3 seconds after laser delivery. Treatment grids of 3×3 or 5×5 laser spots were applied with energies of 20%, 25%, 30%, 40%, and 100% according to the EpM algorithm. An additional 114% energy point was added by increasing laser power without changing the 20-ms pulse duration. Intense marker burns were applied to outline the treatment areas and help locate nondamaging treatment patterns in subsequent analysis. Treatment was applied 7 hours before euthanasia for detection of acute HSP expression and viability staining. For tissue pathology and scanning electron microscopy, animals were euthanized 1 day and 1 hour after laser treatment, respectively, for best detection of structural changes. Immunohistochemistry to detect long-term expression of GFAP was done at 4 weeks.

Damage Threshold Determination

For viability staining, the eye was enucleated immediately after euthanasia, the anterior segment of the globe was removed, and the retina was manually peeled off of the RPE. The RPE–choroid–sclera sample was rinsed briefly in balanced salt solution (BSS) and then immersed in 2 μM calcein AM/12 μM EthD-III (Viability/Cytotoxicity Assay; Biotium, Hayward, CA, USA) solution for 30 minutes in a covered petri dish. Tissue samples were promptly imaged with fluorescence microscopy.

For histologic analysis, eyes were fixed in 1.25% glutaraldehyde/1% paraformaldehyde in cacodylate buffer (pH 7.2) overnight at room temperature. The tissue was then postfixed in osmium tetroxide, dehydrated with a graded series of ethanol, and processed with propylene oxide. Tissue was embedded into epoxy resin (Embed 812; Electron Microscopy Sciences, Port Washington, PA, USA). One-micrometer sections for light microscopy were cut on an ultramicrotome (Reichert-Jung Ultracut E; Leica, Deerfield, IL, USA), stained with toluidine blue, and photographed on a light microscope (Eclipse E1000; Nikon, Tokyo, Japan).

For scanning electron microscopy (SEM) analysis, the sclera, choroid, and RPE were fixed in 1.25% glutaraldehyde/1% paraformaldehyde in 0.2 M sodium cacodylate buffer at room temperature for 30 minutes. The tissue was then fixed for an additional 18 hours at 4°C, rinsed in cacodylate buffer, and postfixed in 1% osmium tetraoxide in 0.2 M cacodylate buffer (pH 7.4). The tissue was washed with distilled water, dehydrated in a series of ethanols, critical point dried, mounted on stubs, and plasma coated with Au/Pd (Denton Vacuum,

Moorestown, NJ, USA). Samples were imaged with a Hitachi S-3400N VP-SEM (Hitachi, Pleasanton, CA, USA).

Immunohistochemistry

For whole-mount immunostaining of the RPE for HSP70 expression, the sclera, choroid, and RPE were fixed in HistoChoice MB tissue fixative (Amresco LLC, Solon, OH, USA) for 4 hours at room temperature. The tissue was then washed in phosphate-buffered saline (PBS) and blocked for 1 hour at room temperature in PBS containing 5% normal goat serum. The tissue was incubated in 0.027 mg/mL mouse mAb anti-HSP70/72 (C92F3A-5, no. ADI-SPA-810-F; ENZO Life Sciences, Farmingdale, NY, USA) in PBS containing 1% normal goat serum at 4°C overnight. This was followed by three 15-minute washes in PBS and incubation in PBS containing 0.027 mg/mL CF594 goat anti-mouse IgG (H+L) secondary antibody (cat. no. 20111; Biotium) for 1 hour at room temperature. The tissue was then washed three times for 15 minutes in PBS. The RPE and choroid were carefully separated from the sclera, mounted with glycerol mounting medium (ab188804; Abcam plc, Cambridge, UK), and imaged with a confocal microscope (Leica SP8 WLL; Leica Microsystems, Inc., Buffalo Grove, IL, USA).

To study long-term expression of GFAP, eyes were enucleated 4 weeks after laser treatment and fixed in 4% paraformaldehyde with 5% sucrose. Samples were processed and embedded in paraffin, and slides were prepared with 5-μm sections. Tissue sections were deparaffinized and high-temperature antigen retrieval (85–90°C) was performed in EDTA (pH 9) buffer for 1 hour. Bovine serum albumin (BSA, 10%) was used as blocking solution for 1 hour at room temperature. Sections were labeled with primary antibody raised against GFAP (SC-6170, goat polyclonal), which is activated in Müller cells in response to retinal injury. The antibody was diluted to 1:25 with PBS/Triton with 1% BSA, and slides were incubated overnight at 4°C. Slides were rinsed in PBS/Triton, incubated with 1:200 FITC (SC-2024) at room temperature for 1 hour, washed again with PBS/Triton, and stained with a fluorescent DNA stain (DAPI). Vectashield mounting medium (H-1000; Vector Laboratories, Inc., Burlingame, CA, USA) was used and sections were imaged with a fluorescent microscope (Nikon Eclipse TE300).

Computational Modeling

A finite-element model of 532-nm laser heating of the rabbit retina published by Sramek et al.[20] was adapted for 577 nm and used to predict temperature rise and tissue response using the Arrhenius damage integral. The adapted model, implemented with a computational package (COMSOL Multiphysics 5.0; Natick, MA, USA), reduces the absorption coefficients in the pigmented layers by 25% to account for lower melanin absorption at 577 nm while increasing absorption coefficients in vascular layers by 25% to account for higher hemoglobin absorption.[27] Using the most common experimental titration value in rabbits, the power producing barely visible burns (100% EpM energy setting) was calculated with 70 mW for 20-ms pulse and 140-μm beam, corresponding to the beam size on the rabbit retina. The EpM algorithm was used to calculate lower energy settings (20%, 25%, 30%, 40%) while higher energy setting (114%) was calculated by increasing the power. The Arrhenius damage integral was calculated as follows:

$$\Omega(\tau) = A \int_0^\tau \exp\left(-\frac{E^*}{R \cdot T(t)}\right) dt$$

Previous correlation of Arrhenius damage integrals and HSP expression[14,22] suggested that Arrhenius values of $\Omega = 0.1$ and

$\Omega = 1$ are the key reference points, where HSP expression and cell damage, respectively, are predicted to begin. One unmeasured parameter, the total transmission of the laser through the eye to the retina, was adjusted to 62% to match the diameter of HSP expression ($\Omega = 0.1$) at 30% energy setting.

Patient Selection

This was a prospective, nonrandomized, interventional case series approved by the Ethics Committee of the Hospital de Clínicas de Porto Alegre, Federal University of Rio Grande do Sul, and adhered to the tenets of the Declaration of Helsinki. Patients were older than 18 years of age, with CSCR and symptoms presented for more than 4 months or macular telangiectasia type 2 (MacTel). The CSCR was confirmed by the presence of one or more leakage points in the fluorescein and/or indocyanine green angiography, subretinal fluid in the optical coherence tomography (OCT) (Spectralis; Heidelberg Engineering, Heidelberg, Germany) and increased choroidal thickness in the enhanced depth imaging (EDI) OCT mode. Macular telangiectasia was diagnosed by bilateral typical appearance of telangiectasic vessels temporal to the fovea on fluorescein angiography with late leakage and OCT. Best-corrected visual acuity (BCVA) measured by the Early Treatment Diabetic Retinopathy Study (ETDRS) protocol was in the range from 20/20 to 20/400. Patients included in the study did not have any other retinal or choroidal disease that could present with similar characteristics. They also had not had prior macular laser treatment, or intravitreal steroids within the last 4 months, or anti-VEGF treatments during the last month prior to the laser treatment. Patients were not eligible if they had either retinal thickening due to the epiretinal membrane or vitreomacular traction syndrome or had undergone major ocular surgery (including cataract surgery) within 6 months.

Treatment Procedures and Evaluation of the Therapeutic Effect

The baseline examination included ETDRS BCVA, slit-lamp examination of the anterior segment, indirect ophthalmoscopy, color fundus photography using CR-2 retinal camera (Canon U.S.A., Melville, NY, USA), fluorescein angiography (FA), and fundus autofluorescence (FAF) using HRA-2 (Heidelberg Retina Angiograph; Heidelberg Engineering). Baseline macula and choroidal thickness and presence of the subretinal fluid were evaluated by OCT (Spectralis). Subfoveal choroidal thickness was defined as the distance from the outer edge of the hyperreflective RPE in the center of the fovea to the inner sclera, using the Spectralis built-in linear measuring tool.

Patients eligible for the therapy received the laser treatment as described below; ETDRS BCVA and central macular thickness (CMT) measurements by OCT were performed monthly for 12 months of follow-up. Fluorescein angiography was repeated after 3, 6, and 12 months. Laser treatment could be repeated up to every 3 months if subretinal fluid persisted or recurred. The effect of the laser treatment was measured by the improvement in visual acuity, assessment of serial retinal autofluorescence, resolution of the retinal detachment and/or subretinal fluid by OCT, and evaluation of leakage areas on FA. Potential adverse events have been monitored with visual acuity, clinical examination, FA, and OCT. In MacTel patients, retreatment could be performed every 6 months if disease was progressing or persistent lacunae remained.

Clinical Laser Settings and Endpoint Management Algorithm

PASCAL laser (Topcon Medical Laser Systems) with 577-nm wavelength and 200-μm retinal spot size was applied via the Area Centralis HD contact lens (Volk Optical, Mentor, OH, USA). Treatment was based on OCT macular thickness map and on the increased autofluorescence area, which included areas of thickened and nonthickened retina. Retinal treatment begins with titration of the laser power to a minimally visible retinal lesion endpoint outside vascular arcades. As ophthalmoscopic visibility of the lesion changes over time, its appearance must be evaluated at a consistent time point after the laser application. For practical clinical usability, evaluation time point of 3 seconds was defined for this protocol. During titration, pulses of 15-ms duration have been used. The titration pulse energy corresponding to a minimally visible burn was assigned the 100% on EpM settings, and the treatment pulse energy was then defined as a percentage of this titration energy. Each energy level corresponds to a unique pair of laser power and pulse duration as described previously.[21]

Treatment was performed at 30% energy, the level established as the highest nondamaging setting in animal studies.[21] Graphic user interface of the EpM allows keeping some of the corner spots of the pattern at 100% energy to produce visible landmarks for orientation. Treatment was initially applied using the round macular grid pattern ($r_{in} = 500$ μm, $r_{out} = 3000$ μm) with landmarks on, using 0.25-diameter spacing between the laser spots. To expand the treated area, additional 2×2 patterns were applied without landmarks inside the inner radius of the macular grid, and 3×3 patterns without landmarks were applied outside the grid. Laser patterns covered both the thickened and nonthickened retina in the posterior pole as determined by the OCT and by increased autofluorescence. During retreatments, all the landmarks were turned off.

Statistical Analysis of Clinical Data

For statistical analysis, the visual acuity data were converted to logarithm of the minimum angle of resolution (logMAR). All clinical data were reported as mean $\pm$ standard error of mean (SEM). The Wilcoxon signed rank test was performed to assess significance of the change in visual acuity and retinal thickness compared to the baseline. Average values of the retinal thickness and visual acuity are plotted with the error bar representing the standard error of the mean.

RESULTS

Preclinical Studies of Nondamaging Hyperthermia

Damage to the RPE cells after laser exposure in rabbit eyes was checked using three methods: viability/cytotoxicity staining (Biotium), histology, and SEM. For viability/cytotoxicity staining, four eyes were treated with a total of 250 laser spots at 30% energy, 250 spots at 40%, and 54 spots at 100%. At 30% energy, none of the laser spots showed any dead cells. An example of the pattern area with no visible changes is shown in Figure 2A. At 40% energy, damage was visible in 69% of the laser spots. Figure 2B presents a part of the 5×5 pattern at 40% energy, with dead RPE cells seen with EthD-III fluorescent red–stained nuclei. At 100% energy, all of the laser spots resulted in RPE cell death. The 3×3 pattern in Figure 2C has red nuclei, as well as RPE cells that are missing entirely. The hazy red seen in several spots arises from out-of-focus staining of dead photoreceptors fused onto the RPE.

Histology of the retina lasered 1 day before enucleation shows unblemished tissue at 30% (Fig. 2D), slight damage in the 50% area delineated by yellow arrows (Fig. 2E), and clearly damaged 100% area (Fig. 2F) with outer segments fused to the RPE and pyknotic nuclei in the outer nuclear layer. Scanning
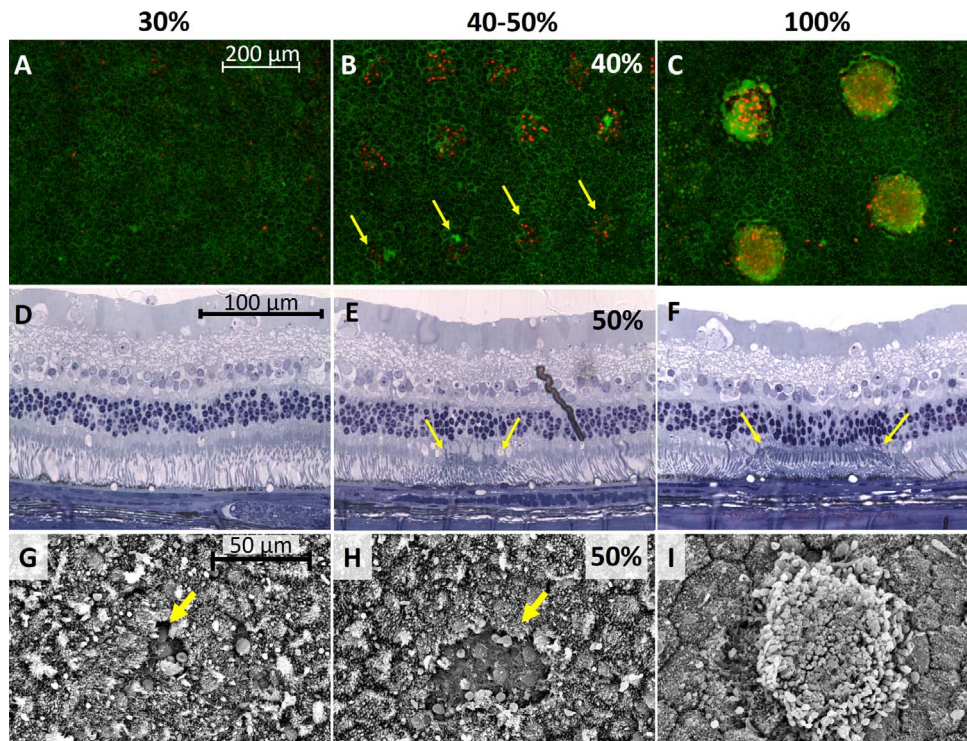
FIGURE 2. Determination of damage threshold. (**A–C**) Viability/cytotoxicity-stained RPE cells 7 hours after laser treatment at 30%, 40%, and 100% energy setting in rabbits. (**D–F**) Histology of retina and RPE 1 day after laser treatment at 30%, 50%, and 100% energy. (**G–I**) Scanning electron microscopy of RPE 1 day after laser treatment at 30%, 50%, and 100%.

electron microscopy shows similar results, with undisturbed RPE at 30% energy except for a single cell indicated by the yellow arrow in Figure 2G, while 50% energy produced a larger damage zone (Fig. 2H). At 100% energy the outer segments were fused onto the RPE (Fig. 2I). Results from all three methods of analysis indicate that the 40% energy setting or greater is damaging while below 30% is nondamaging.

HSP70 Expression

Confocal microscope images of immunostained RPE with laser patterns of 20%, 25%, 30%, 40%, 100%, and 114% energy were analyzed for expression of HSP70. No expression was observed at 20% energy from a total of 250 observed laser spots. For 25% energy ($n = 200$), 57% of laser spots showed HSP70 expression while 30% energy ($n = 238$) and 40% energy ($n = 150$) had 98% and 99% expression, respectively. All laser spots at 100% ($n = 54$) and 114% ($n = 54$) had HSP expression. Figures 3a through 3c show patterns of laser spots at 25%, 30%, and 40% energy, where each spot produces a disc of activated cells. In contrast, at the 100% energy setting, expression occurs in a ring of cells as can be seen in Figure 3D.

In each image, the expression areas were measured by outlining the boundaries with elliptical lines, with the dotted and solid lines indicating the outer and inner limits, where applicable. The HSP expression areas were measured for all immunostained laser spots, and damage zone diameters were measured for viability/cytotoxicity-stained samples. The mean values for each laser setting are plotted as an average area per 100 delivered laser spots in Figure 3E, along with predicted expression areas from the computational model. Error bars indicate the expression areas corresponding to the 25th and 75th percentiles. The distribution of outer expression diameters, given as the geometric mean of the major and minor axes of the ellipse, is plotted in histograms in Supplementary Figures S1A and S1B for damage and HSP expression, respectively.

A computational model of laser heating of the retina was used to estimate the temperature rise during treatment. Supplementary Figure S2 shows thermal maps of peak temperature rise for 30% (Supplementary Fig. S2A) and 100% (Supplementary Fig. S2B) settings and the maximum RPE temperature course for 25%, 30%, 40%, and 100% settings (Supplementary Fig. S2C). Arrhenius integrals were calculated from these temperature courses to predict the size of the damage area ($\Omega > 1$) and HSP70 expression area ($0.1 < \Omega < 1$). These are plotted for the experimentally measured settings in Supplementary Figure S3, with the dotted lines outlining the areas of HSP expression and solid lines outlining areas of damage. The ring pattern of HSP expression at 100% settings illustrates the fact that dead RPE cells do not express HSP, thereby defining the upper bound of $\Omega < 1$. Figure 3E plots the total expression area and total damage area per 100 laser spots, as predicted by the model. For example, with the 30% energy setting and 200-μm spots, the predicted expression area is 0.71 mm^2 per 100 spots.

Glial Fibrillary Acidic Protein Expression

Glial fibrillary acidic protein expression associated with activation of glial cells after retinal photocoagulation is known to peak around 1 month and disappear 4 months after the treatment.[25] To check whether Müller cells are also activated by nondamaging thermal treatment, we applied immunohistochemistry targeting GFAP at 1 month after laser treatment. As shown in Figure 4, the 30% laser spot shows elevated expression of GFAP in Müller cells in the center of the laser spot, with no visible damage to the outer nuclear layer. The 100% laser lesion shows highly increased expression of GFAP in Müller cells across a larger part of the laser area, which extends down into an area of photoreceptor damage. Activation extends to the right of the treatment spot in both images due to proximity to the next spot (not visible in these photos).
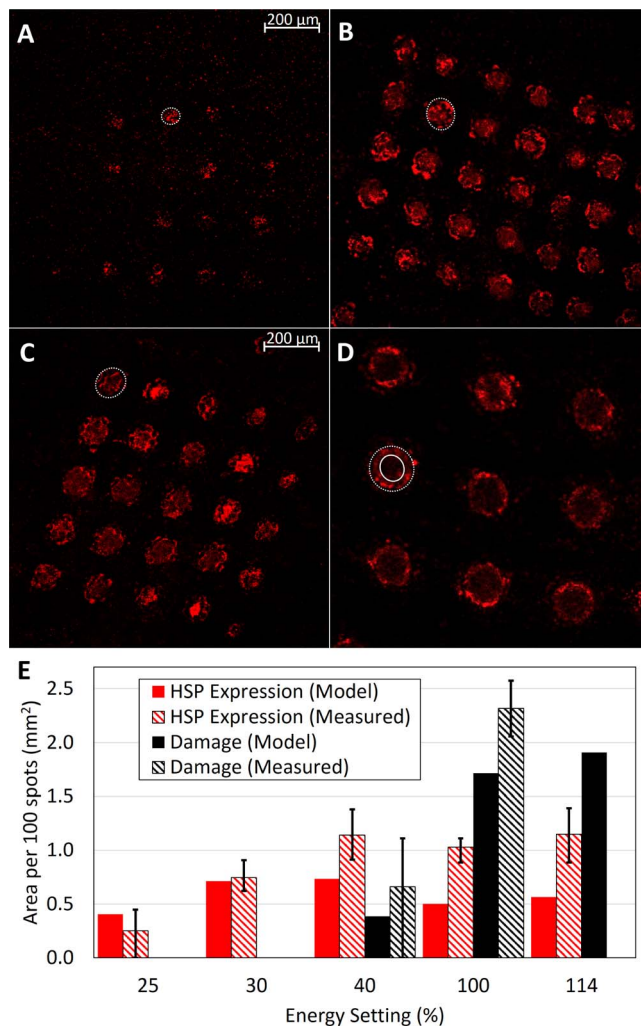
Investigative Ophthalmology & Visual Science

FIGURE 3. HSP70 expression in RPE. Expression area 7 hours after laser treatment at (**A**) 25%, (**B**) 30%, (**C**) 40%, and (**D**) 100% energy. Expression area is indicated by *dotted lines*. In 100%, *solid line* indicates inner limit of HSP70 expression. (**E**) Average expression (*red*) or damage (*black*) area per 100 spots for 25% ($N_{HSP} = 200$), 30% ($N_{HSP} = 238$, $N_{damage} = 250$), 40% ($N_{HSP} = 150$, $N_{damage} = 250$), 100% (N_{HSP} $N_{damage} = 54$), and 114% ($N_{HSP} = 54$) energy. *Solid bars* show model predictions while *striped bars* depict experimental measurements. *Error bars* on experimental measurements give interquartile (25%–75%) range.

Based on these results, we defined the laser settings for clinical testing at the upper bound of the nondamaging regime—30% energy on the EpM scale. To maximize the tissue response and associated clinical efficacy, we decided to apply patterns with much higher spot density than in conventional photocoagulation: Spots were separated by 0.25 diameters rather than 2 diameters in the conventional macular grid. Unlike conventional photocoagulation associated with retinal damage, NRT enables high-density treatment due to lack of tissue damage, which might result in much higher clinical efficacy than conventional photocoagulation, among other benefits.

Clinical Results With CSCR

To study the clinical efficacy of NRT in treatment of chronic CSCR, 21 eyes from 20 patients (15 male and 5 female) with chronic CSCR were enrolled. To exclude patients with high potential for spontaneous resolution of the subretinal fluid,

only patients with at least 4 months of symptoms were enrolled, and the mean duration of CSCR prior to the treatment was 11 ± 4 months. The average age on enrollment was 56 ± 17 years. Typical power range in titration with 200-μm spot diameter and 15-ms pulses was 90 to 150 mW, with an average of 126 ± 14 mW. Treatment was performed using 30% of the titration energy, with 0.25-diameter spot spacing in all the PASCAL patterns: macular grid, 2×2 and 3×3 square patterns. A graphical user interface for adjustment of the laser parameters is shown in Figure 5A. The average number of spots per treatment was 548 ± 212. The treatment spots applied at 30% energy settings could not be detected clinically, nor by OCT, FAF, or FA at any time point during the 12-month follow-up. Autofluorescence image of the fundus 1 month after the treatment reveals the titration spots below the arcade (pointed to by white arrows in Fig. 5B) and landmark burns (100% energy) in the macular grid (pointed to by black arrows in Fig. 5B). None of the other treatment locations are visible.

One example of a response to NRT in a CSCR patient is shown in Figure 6. In this particular case, the 61-year-old patient had had chronic CSCR for more than 6 months and presented with serous retinal detachment and visual acuity of 20/60. Thickness of the choroid at baseline was 165 μm, as indicated by yellow bar in Figure 6A. One month after the treatment, the CMT decreased significantly and visual acuity increased to 20/30. Choroidal thickness decreased to 145 μm as shown in Figure 6B. After two treatments, subretinal fluid completely resolved and visual acuity improved to 20/20. Choroidal thickness reached 135 μm as shown in Figure 6C. Two other clinical examples demonstrating effective resolution of subretinal fluid are presented in Supplementary Figures S4 and S5.

On average, CMT decreased following laser treatment from 362 ± 11 to 283 ± 9 μm ($P = 0.001$) (Fig. 7A). In 81% of patients, the subretinal fluid was completely resolved, and in 19% there was only minimal fluid left. Choroidal thickness also decreased after laser treatment. Average subfoveal choroidal thickness at baseline was 349 ± 20 μm. It decreased to 290 ± 15 μm after 3 months and remained stable over 1-year follow-up (Fig. 7B), with a final thickness of 293 ± 17 μm at 12 months ($P = 0.005$). Patients with complete resolution of subretinal fluid on OCT had no leakage on FA. In patients with partial resolution of the fluid, some residual hyperfluorescence could still be observed. Patients gained, on average, 12.2 ± 3.0 ETDRS letters in BCVA at 2 months, which remained steady by 12 months (12.5 ± 4.0, $P < 0.001$) as shown in Figure 7C.

Subretinal fluid resolved in 16% of patients after one treatment, while 58% required one retreatment after 3 months due to either recurrent fluid or incomplete fluid resolution. Sixteen percent of patients received a second retreatment, and the remaining 10% received a third retreatment, that is, a total of four laser treatments, as summarized in the Table. The average number of treatments was 2.2 per eye. There were no adverse events related to the treatment. No visible laser marks at the 30% treatment settings could be detected either by clinical observation, OCT, FAF, or FA during 12 months of follow-up. There were also no visible marks of any cumulative retinal damage after retreatments.

Clinical Results With MacTel

Ten eyes of five patients (one male and four females) with MacTel type 2 (acquired and bilateral) and an average age of 56 ± 17 years were enrolled in the study. Typical power in titration with 200-μm spot diameter and 15-ms pulses was 120 mW, varying from 100 to 140 mW. Treatment was performed using 30% of the titration energy and 0.25-diameter spot spacing in all the PASCAL patterns: macular grid, 2×2 and $3 \times$
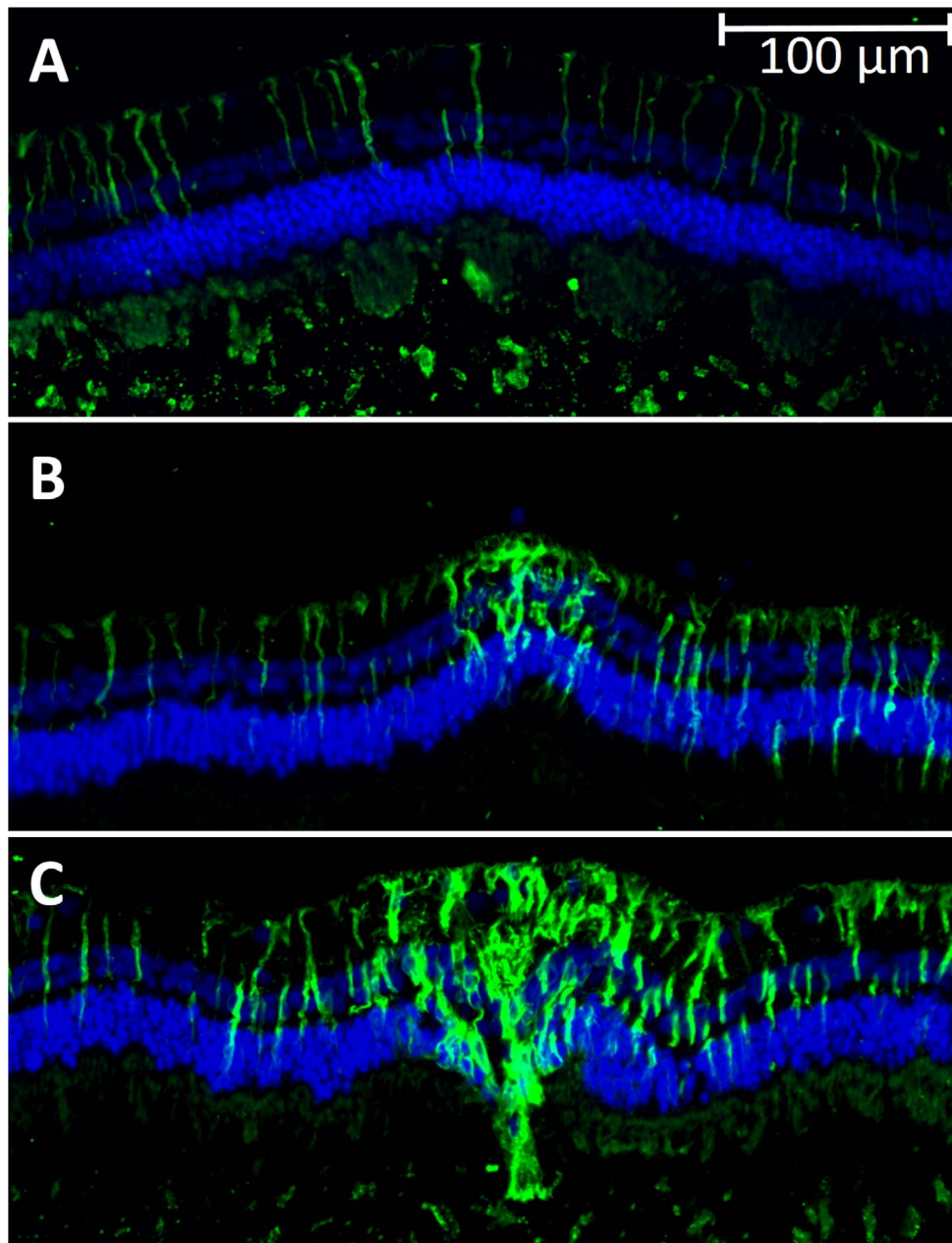
FIGURE 4. GFAP expression in the retina. GFAP expression in the retina 4 weeks after laser treatment. *Green* fluorescent marker indicates GFAP activation, while *blue* is DAPI staining of the nuclei. (**A**) Control area shows low background level of GFAP; (**B**) 30% laser lesion with GFAP expression in the inner retina; (**C**) 100% laser lesion with wider GFAP expression throughout the retina. Expression extends to the *right* of the lesion due to proximity to the next spot in the pattern (not visible in this photo).

3 square patterns. The average number of spots per treatment was 382. The treatment spots applied at 30% energy settings could not be detected clinically or by OCT, FAF, or FA. After 1 month, some hyperreflective spots could be seen with infrared imaging; however, FAF, OCT, and FA did not show any damage to outer or inner retina.

Unlike the natural course of MacTel, which leads to thinning of the central macula due to loss of photoreceptors,[28] the average CMT in the treated eyes was stable during the 12-month follow-up period: It went from 246 ± 13 μm at baseline to 241 ± 14 μm ($P = 0.48$) at 1 year. The inner and outer retinal lacunae significantly decreased in 80% of the eyes, while the central outer nuclear layer thickness remained the same as at baseline, 68 ± 6 vs. 69 ± 8 μm, suggesting that the decreased cavitation was not due to collapsed tissue as usually happens with the natural progression of MacTel.

An example of intraretinal lacunae reduction by 50% in area is shown in Supplementary Figure S6: It went from 0.08 mm² at baseline (Supplementary Fig. S6A) to 0.04 mm² at 12 months (Supplementary Fig. S6B). In another patient, the outer nuclear layer and the inner segment/outer segment (IS/OS) junction line were completely missing at baseline (Figs. 8A–C). Five months after treatment, and subsequently through the 12-month follow-up period, the outer nuclear layer was partially restored, with the external limiting membrane (Fig. 8D) and IS/OS line (Fig. 8E) reappearing. The detailed retinal thickness maps of this patient are shown in Supplementary Figure S7. In two eyes of one patient with the most severe degeneration, the
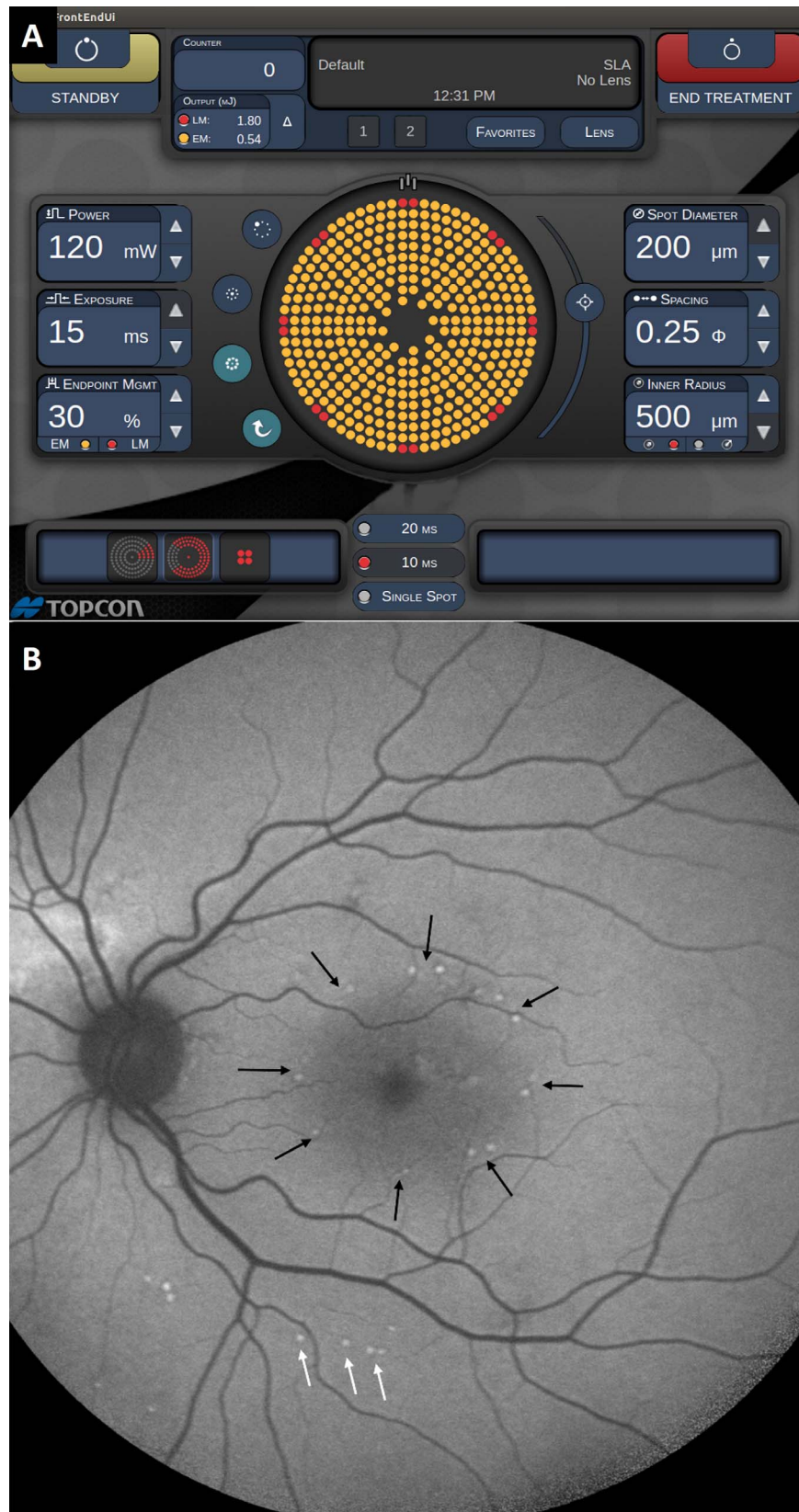
FIGURE 5. Nondamaging retinal laser therapy with Endpoint Management. (**A**) Graphic user interface of the EpM software on Streamline PASCAL. *Red dots* indicate the landmarks (100% energy, optional). *Yellow dots* indicate the locations to be treated at 30% energy. (**B**) Fundus autofluorescence 1 month after NRT with landmarks that appear as spots with increased FAF (*black arrows*). Titration points are also visible in FAF outside the arcades (*white arrows*). The 30% treatment spots were not visible clinically by OCT or FAF.
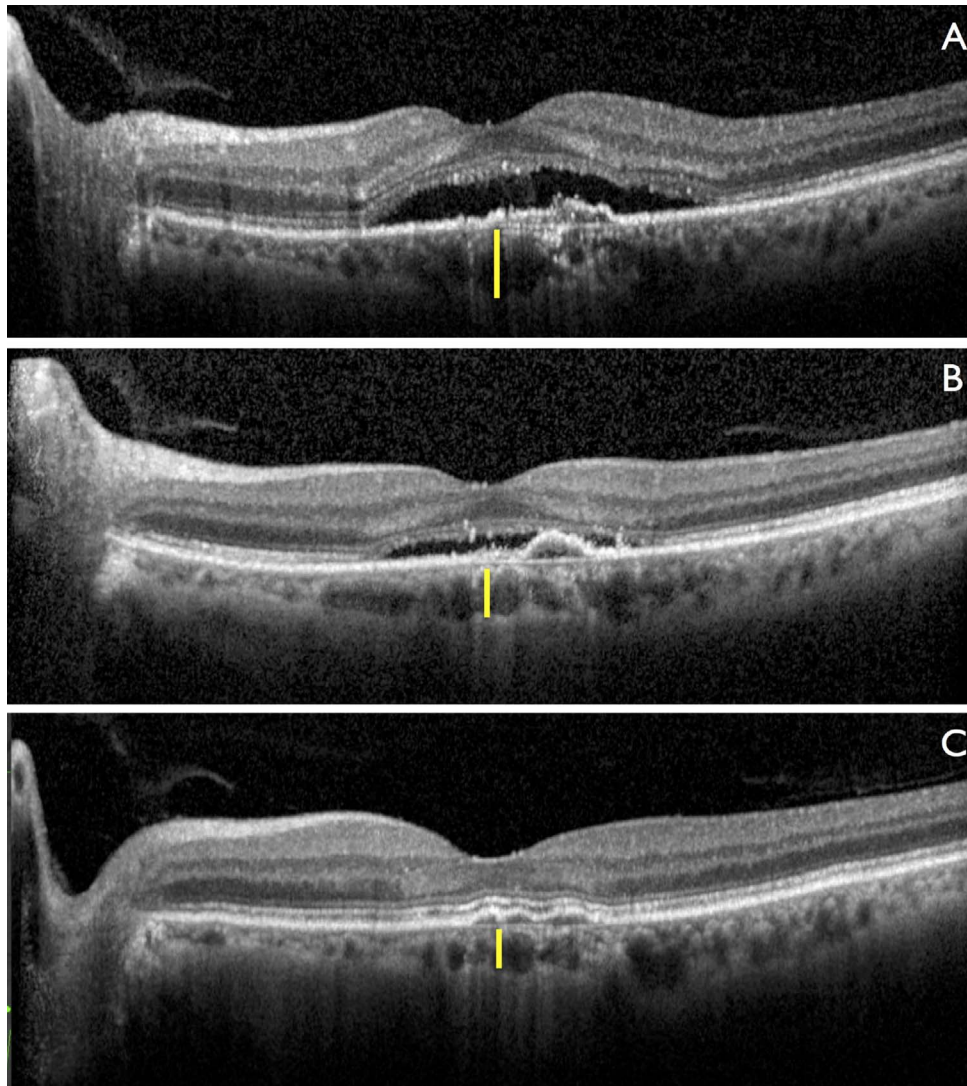
FIGURE 6. Retinal response to NRT in patient with chronic CSCR. (**A**) Chronic serous retinal detachment with RPE irregularities, visual acuity (VA) of 20/60. (**B**) Decrease in central macular thickness (CMT) and increase of visual acuity to 20/30 1 month after treatment. (**C**) Complete resolution of subretinal fluid, with VA of 20/20, which remains stable for 1 year. *Yellow vertical bars* indicate subfoveal choroidal thickness, which decreased from 165 to 135 µm.

lacunae did not decrease significantly, but the retina remained stable for 1 year. There were no signs of disease progression or further loss of photoreceptors throughout the follow-up in any of the treated eyes. Visual acuity improved, on average, from 20/40 at baseline to 20/25 at 1 year. Four out of 10 patients were retreated once during the follow-up period due to persistent lacunae.

DISCUSSION

Preclinical animal studies using the EpM algorithm were performed to determine the safe therapeutic window and tissue response to hyperthermia. Figure 1 shows the titration point and predicted therapeutic window (shaded in green) based on the computational model of the retinal heating. Areas colored in red correspond to damaging settings, those in green to the nondamaging therapeutic range, and blue indicates subtherapeutic. According to this plot, the damage threshold $\Omega = 1$ crosses the EpM line (solid black) at 40%. Our experimental results with viability/cytotoxicity staining confirmed that the

damage threshold begins at 40% energy. Across four eyes in three animals, 40% energy settings were damaging in 69% of the 250 total delivered spots. The damage area increased with energy, as shown in Figure 3E, and error bars indicate that tissue response can vary, likely due to pigmentation fluctuation across the eye. Nonetheless, treatments at 30% energy were uniformly nondamaging following 250 experimental spots in four different eyes, suggesting that this setting (in the middle of the green zone) is sufficiently below the damage threshold to account for normal pigment variation.

Heat shock protein expression in rabbits was observed above 25% settings (Fig. 3E), which indicates that 25% energy is the lower limit to the therapeutic window of NRT—a little higher than the 20% predicted by the model. The HSP activation area increased with energy up to 40%, but not beyond that, since at higher energies the area of expression became donut-shaped, with a dark center due to tissue damage. Only the cells at the "warm" edges of the hot coagulating spot survived the hyperthermia and expressed HSP. Therefore, increasing laser energy above the damage threshold is not expected to improve the therapeutic response. Instead,
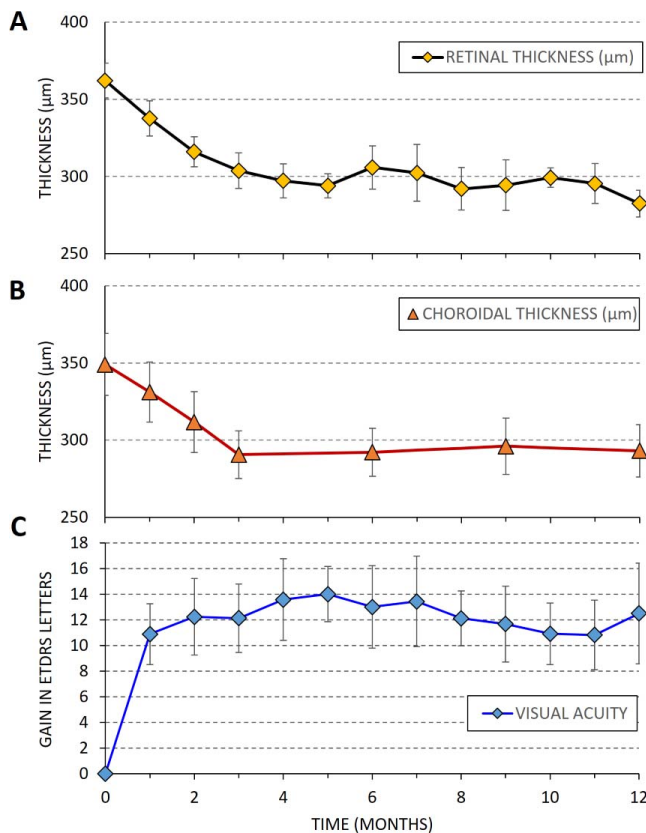
FIGURE 7. Twelve-month follow-up after NRT in CSCR patients ($N = 21$ eyes). (**A**) Central macula thickness. (**B**) Subfoveal choroidal thickness. (**C**) Gain in visual acuity (BCVA in ETDRS letters). *Error bars* represent the standard error of mean.

TABLE. Number of Treatments in Patients During the 12-Month Follow-Up Period

Number of treatments	1	2	3	4
Fraction of patients, %	16	58	16	10

that there is no tissue damage in sufficiently long follow-up. The current study validated the lack of tissue damage, and we now feel comfortable decreasing the spot spacing to 0, especially in retreatment. However, we do not recommend starting with such a tight spacing since titration criteria (visibility of the lesion) may vary between physicians.

It is also important to emphasize that since the overarching goal was the development of an algorithm for nondamaging laser therapy of the macula, we have chosen a conservative approach and titrated the laser in the periphery (beyond the arcades), where the retinal coagulation threshold is lower than in the macula. Areas of enhanced scattering (edema) and reduced pigmentation will also experience lower temperature rise and the tissue response will be diminished accordingly. However, we prefer occasional undertreatment rather than local titration in the macula, which will produce tissue damage. Results of this trial confirm that despite these conservative settings, NRT was effective in treatment of chronic CSCR and MacTel, without tissue damage.

Mechanisms of action leading to therapeutic benefits remain to be explored in more detail. Protein misfolding and aggregation in cells is a fundamental component of aging.[29] Normally, HSPs refold the damaged proteins and thereby protect cells from protein aggregation and associated proteotoxicity.[30] However, transcriptional pathways, including heat shock factor (HSF1) potency, decline in aging cells,[31] leading to a decrease in protein quality control, which in turn contributes to protein aggregation commonly observed in neurodegenerative diseases.[32] Induction of HSP in aging cells helps maintain the protein homeostasis by refolding the damaged proteins, thereby promoting longevity and rejuvenating cellular functions. In addition, molecular chaperones such as HSP27 and HSP70 have antiapoptotic functions and can prevent depletion of essential cell populations in degenerative processes.[33] Therefore, enhanced synthesis of HSP and co-chaperones in RPE in response to laser-induced thermal stress might bring back normal physiology of these cells in aging and disease, including enhanced capability of fluid pumping from the retina and decrease in choroidal permeability.

Our results demonstrate significant reduction, and in a majority (81%) of chronic CSCR patients, a complete resolution of subretinal fluid, with corresponding improvement in visual acuity. These outcomes are very different from the natural course of chronic CSCR, which does not spontaneously resolve in the majority of cases and usually progresses to further decrease in visual acuity and morphologic damage to photoreceptors.[16,34] Nondamaging retinal therapy produced no observable retinal damage at any of the follow-up time points except for the visible landmarks, which remained visible in IR and AF imaging. Recurrence of the intraretinal fluid occurred in several patients after a few months, which indicates that the improvement provided by NRT may fade over time. However, retreatment with the same parameters was found to be safe and effective, and no cumulative retinal damage was detected over the follow-up period. Retinal response to retreatment was similar to that for the first treatment, and in some cases even better than the initial result. One reason for better response to retreatment could be simply the fact that retreatment was applied to much less edematous retina than the first treatment. Reduced light scattering in this
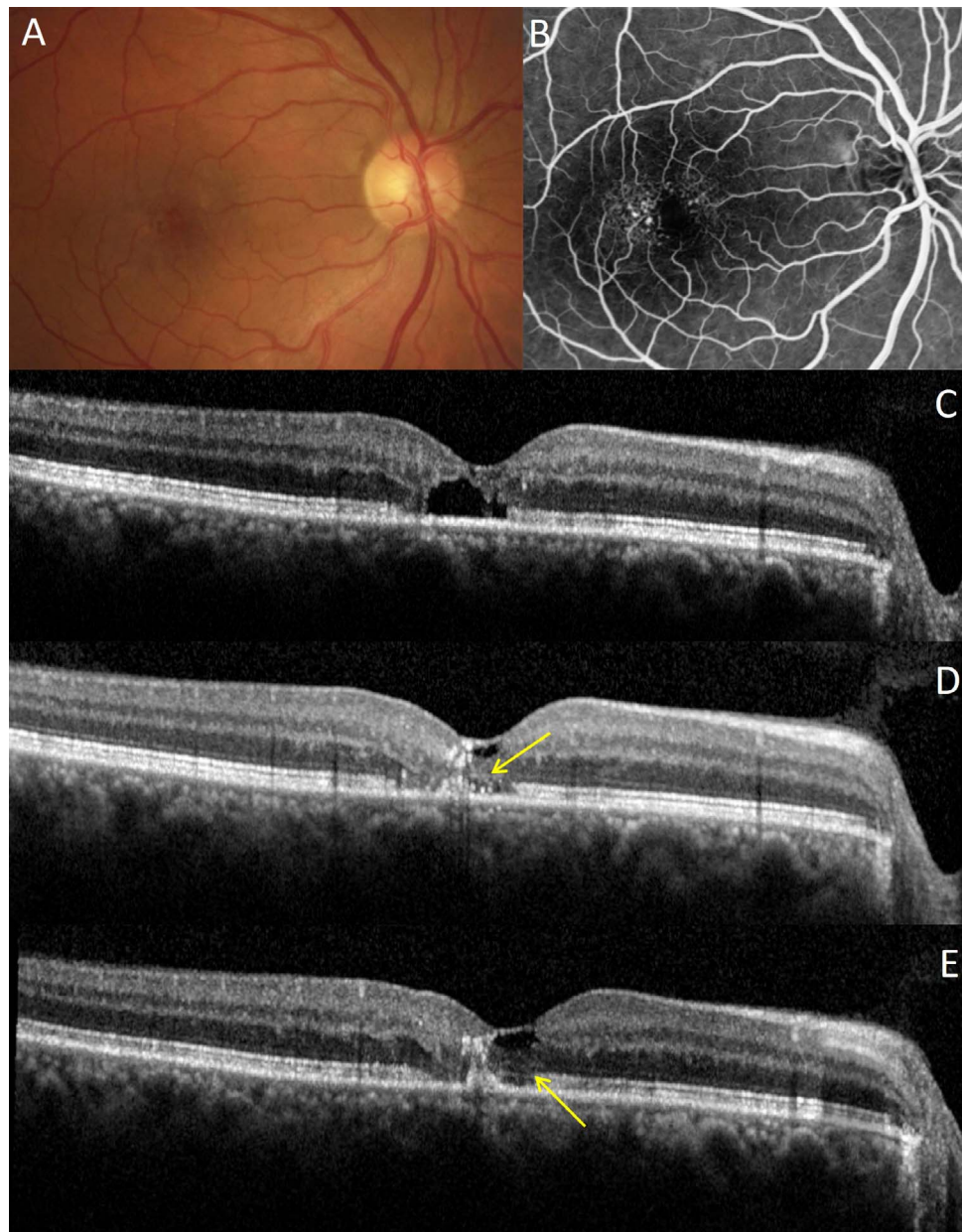
it just adds a damage zone in the center of the laser lesion, which increases with energy, as can be seen in Figure 3E.

Experimentally, the HSP expression area and the damage zone at 40%, 100%, and 114% were larger than computed with the model (Fig. 3E), likely due to the cell size aliasing effect, where an entire RPE cell is activated or damaged even if only a part of it falls in the HSP expression zone or damage zone. Given that the modeled expression zones at 100% and 114% are approximately 20 μm in width (Fig. S3) and RPE cells are of a similar size, partial overlap of the cells with the activation area or damage zone would increase the observed expression area. Despite this discrepancy, the model is useful for understanding the activated HSP expression area and validating the EpM methodology.

Activation area at 30% is a little smaller than the maximum response (at 40% and beyond), but lack of tissue damage allows application of much denser patterns than one could afford with conventional damaging photocoagulation. For example, a pattern with edge-to-edge spot spacing of 0.25-diameter would cover 50% of the scanned area, while a pattern with 0 spacing would cover 79% of the area. This is significantly more coverage than with a conventional macular grid using 2-diameter spacing, which only exposes 9% of the scanned area. Such dense coverage is likely to boost the therapeutic response.

Based on these studies, the laser settings for the NRT were set at 30% energy to operate in the middle of the safe therapeutic window and avoid tissue damage due to occasional variations of pigmentation. To maximize the therapeutic response, the spot spacing was set at 0.25 spot diameter. In principle, it could be decreased to 0, but only after validating

FIGURE 8. Retinal response to NRT in MacTel patient. (**A**) Baseline fundus color image. (**B**) Baseline fluorescein angiography with typical telangiectasic vessels temporal to fovea. (**C**) Baseline OCT image with subfoveal cavitation and loss of IS/OS junction line integrity. (**D**) Partial restoration of outer nuclear layer and external limiting membrane (*arrow*) at 5 months; (**E**) at 12 months, the IS/OS junction line became more visible (*arrow*).

case would increase the temperature rise and improve therapeutic response.

Macular telangiectasia type 2 is considered a neurovascular degenerative disease associated with progressive neuroretinal tissue loss, with an average annual progression of IS/OS break area of 0.140 mm^2,[35] leading to severe visual impairment. Its vascular aspects include telangiectasic vessels, usually temporal to the fovea, and in some cases choroidal neovascularization. Although no precise cause has been determined for this disease, Müller cell depletion has been associated with the classic pathophysiologic findings.[26] Anti-VEGF agents, steroids, photodynamic therapy, photocoagulation, and recently sustained release of the ciliary neurotrophic factor (CNTF)[36] have been tried for MacTel, but none have been found to be effective in treatment of this disease so far.

Unlike natural history or previous therapeutic attempts,[37] our initial results with MacTel patients are very encouraging: We observed a decrease of the intraretinal lacunae and improvement in visual acuity, and we did not detect progression of IS/OS break area or outer retinal degeneration or in choroidal neovascularization during the follow-up period. There even seemed to be some signs of partial restoration of the photoreceptor layer. Activation of Müller cells that we observed in preclinical studies might play a role in this response since contraction of activated Müller cells after conventional photocoagulation was hypothesized to be a driving force behind migration of the photoreceptors into the lesion.[25]

Limitations of these studies include the small number of eyes (21 in CSCR, 10 in MacTel) and absence of a control group; therefore larger controlled clinical trials are being planned. It is important to note, however, that CSCR patients had persistent

conditions for at least 4 months prior to laser treatment (11 months on average), increased choroidal thickness, and signs of chronic RPE damage visible in autofluorescence and OCT. Previous studies demonstrated that chronic CSCR has a very limited resolution rate, with 92% of persistent leakage in the observation-only control group, and therefore treatment is warranted after confirming chronicity of the disease.[16,38]

The EpM algorithm is designed to normalize for pigmentation variations and ocular transparency between individuals by visible titration in each patient prior to treatment. Nevertheless, there is still variation across the retina that is difficult to account for. While we currently recommend 30% as a conservative setting to ensure lack of damage based on clinical observations and preclinical studies, increased therapeutic effect may be possible with slightly higher settings. Recent measurement of the damage threshold in the human eye[39] showed that up to 35% EpM was nondamaging (Peter Karth, oral communication, 2016). Future developments in real-time tissue temperature monitoring, including optoacoustic[40,41] and laser speckle[42] measurements, may allow for precise temperature control of each individual laser pulse. This would allow us to adjust laser settings in every spot and thereby fully compensate for variation in retinal pigmentation and transparency in order to maximize the safety and efficacy of NRT.

In summary, 1-year results with chronic CSCR and MacTel demonstrated that NRT is efficient and safe for treatment of the macula. Success in treatment of two disparate disorders by activation of endogenous repair pathways, indicated by upregulation of HSP in RPE and GFAP expression in Müller cells, suggests that NRT might also be beneficial for treatment of other outer retinal diseases with different pathophysiology, including macular edema and diseases associated with RPE deficiency such as drusen in dry AMD. Lack of tissue damage allows for application of high-density treatment patterns to increase therapeutic response and periodic retreatments for chronic diseases. Availability of the EpM software on the market enables immediate testing of NRT for various macular disorders.

References

1. Photocoagulation treatment of proliferative diabetic retinopathy. Clinical application of Diabetic Retinopathy Study (DRS) findings, DRS Report Number 8. The Diabetic Retinopathy Study Research Group. *Ophthalmology*. 1981;88:583–600.

2. Photocoagulation for diabetic macular edema. Early Treatment Diabetic Retinopathy Study report number 1. Early Treatment Diabetic Retinopathy Study research group. *Arch Ophthalmol*. 1985;103:1796–1806.

3. Burumcek E, Mudun A, Karacorlu S, Arslan MO. Laser photocoagulation for persistent central serous retinopathy: results of long-term follow-up. *Ophthalmology*. 1997;104: 616–622.

4. Argon laser photocoagulation for macular edema in branch vein occlusion. The Branch Vein Occlusion Study Group. *Am J Ophthalmol*. 1984;98:271–282.

5. Brinkmann R, Roider J, Birngruber R. Selective retina therapy (SRT): a review on methods, techniques, preclinical and first clinical results. *Bull Soc Belge Ophtalmol*. 2006;302:51–69.

6. Roider J, Liew SHM, Klatt C, et al. Selective retina therapy (SRT) for clinically significant diabetic macular edema. *Graefes Arch Clin Exp Ophthalmol*. 2010;248:1263–1272.

7. Wood JPM, Shibeeb O, Plunkett M, Casson RJ, Chidlow G. Retinal damage profiles and neuronal effects of laser treatment: comparison of a conventional photocoagulator and a novel 3-nanosecond pulse laser. *Invest Ophthalmol Vis Sci*. 2013;54:2305–2318.

8. Schuele G, Rumohr M, Huettmann G, Brinkmann R. RPE damage thresholds and mechanisms for laser exposure in the microsecond-to-millisecond time regimen. *Invest Ophthalmol Vis Sci*. 2005;46:714–719.

9. Lavinsky D, Chalberg TW, Mandel Y, et al. Modulation of transgene expression in retinal gene therapy by selective laser treatment. *Invest Ophthalmol Vis Sci*. 2013;54:1873–1880.

10. Zhang JJ, Sun Y, Hussain AA, Marshall J. Laser-mediated activation of human retinal pigment epithelial cells and concomitant release of matrix metalloproteinases. *Invest Ophthalmol Vis Sci*. 2012;53:2928–2937.

11. Shukla D, Kolluru C, Vignesh TP, Karthikprakash S, Kim R. Transpupillary thermotherapy for subfoveal leaks in central serous chorioretinopathy. *Eye*. 2006;22:100–106.

12. Reichel E, Berrocal AM, Ip M, et al. Transpupillary thermotherapy of occult subfoveal choroidal neovascularization in patients with age-related macular degeneration. *Ophthalmology*. 1999;106:1908–1914.

13. Benner JD, Ahuja RM, Butler JW. Macular infarction after transpupillary thermotherapy for subfoveal choroidal neovascularization in age-related macular degeneration. *Am J Ophthalmol*. 2002;134:765–768.

14. Luttrull JK, Sramek C, Palanker D, Spink CJ, Musch DC. Long-term safety, high-resolution imaging, and tissue temperature modeling of subvisible diode micropulse photocoagulation for retinovascular macular edema. *Retina*. 2012;32:375–386.

15. Yadav NK, Jayadev C, Mohan A, et al. Subthreshold micropulse yellow laser (577 nm) in chronic central serous chorioretinopathy: safety profile and treatment outcome. *Eye*. 2015;29: 258–264, quiz 265.

16. Roisman L, Magalhães FP, Lavinsky D, et al. Micropulse diode laser treatment for chronic central serous chorioretinopathy: a randomized pilot trial. *Ophthalmic Surg Lasers Imaging Retina*. 2013;44:465–470.

17. Figueira J, Khan J, Nunes S, et al. Prospective randomised controlled trial comparing sub-threshold micropulse diode laser photocoagulation and conventional green laser for clinically significant diabetic macular oedema. *Br J Ophthalmol*. 2009;93:1341–1344.

18. Venkatesh P, Ramanjulu R, Azad R, Vohra R, Garg S. Subthreshold micropulse diode laser and double frequency neodymium: YAG laser in treatment of diabetic macular edema: a prospective, randomized study using multifocal electroretinography. *Photomed Laser Surg*. 2011;29:727–733.

19. Sivaprasad S, Elagouz M, McHugh D, Shona O, Dorin G. Micropulsed diode laser therapy: evolution and clinical applications. *Surv Ophthalmol*. 2010;55:516–530.

20. Sramek C, Paulus Y, Nomoto H, Huie P, Brown J, Palanker D. Dynamics of retinal photocoagulation and rupture. *J Biomed Opt*. 2009;14:034007.

21. Lavinsky D, Sramek C, Wang J, et al. Subvisible retinal laser therapy: titration algorithm and tissue response. *Retina*. 2014; 34:87–97.

22. Sramek C, Mackanos M, Spitler R, et al. Non-damaging retinal phototherapy: dynamic range of heat shock protein expression. *Invest Ophthalmol Vis Sci*. 2011;52:1780–1787.

23. Yenari MA, Liu J, Zheng Z, Vexler ZS, Lee JE, Giffard RG. Antiapoptotic and anti-inflammatory mechanisms of heat-shock protein protection. *Ann N Y Acad Sci*. 2005;1053:74–83.

24. Luttrull JK, Chang DB, Margolis BWL, Dorin G, Luttrull DK. Laser resensitization of medically unresponsive neovascular age-related macular degeneration. *Retina*. 2015;35:1184–1194.

25. Sher A, Jones BW, Huie P, et al. Restoration of retinal structure and function after selective photocoagulation. *J Neurosci*. 2013;33:6800–6808.

26. Powner MB, Gillies MC, Tretiach M, et al. Perifoveal Müller cell depletion in a case of macular telangiectasia type 2. *Ophthalmology*. 2010;117:2407–2416.

27. Sramek CK, Leung L-SB, Paulus YM, Palanker DV. Therapeutic window of retinal photocoagulation with green (532-nm) and yellow (577-nm) lasers. *Ophthalmic Surg Lasers Imaging*. 2012;43:341–347.

28. Krivosic V, Tadayoni R, Massin P, Erginay A, Gaudric A. Spectral domain optical coherence tomography in type 2 idiopathic perifoveal telangiectasia. *Ophthalmic Surg Lasers Imaging*. 2009;40:379–384.

29. Murshid A, Eguchi T, Calderwood SK. Stress proteins in aging and life span. *Int J Hyperthermia*. 2013;29:442–447.

30. Sreekumar PG, Kannan R, Kitamura M, et al. αB crystallin is apically secreted within exosomes by polarized human retinal pigment epithelium and provides neuroprotection to adjacent cells. *PLoS One*. 2010;5:e12578.

31. Hou Y, Wei H, Luo Y, Liu G. Modulating expression of brain heat shock proteins by estrogen in ovariectomized mice model of aging. *Exp Gerontol*. 2010;45:323–330.

32. Gestwicki JE, Garza D. Protein quality control in neurodegenerative disease. *Prog Mol Biol Transl Sci*. 2012;107:327–353.

33. Chopek JW, Gardiner PF. Life-long caloric restriction: effect on age-related changes in motoneuron numbers, sizes and apoptotic markers. *Mech Ageing Dev*. 2010;131:650–659.

34. Nicholson B, Noble J, Forooghian F, Meyerle C. Central serous chorioretinopathy: update on pathophysiology and treatment. *Surv Ophthalmol*. 2013;58:103–126.

35. Sallo FB, Peto T, Egan C, et al. The IS/OS junction layer in the natural history of type 2 idiopathic macular telangiectasia. *Invest Ophthalmol Vis Sci*. 2012;53:7889–7895.

36. Chew EY, Clemons TE, Peto T, et al. Ciliary neurotrophic factor for macular telangiectasia type 2: results from a phase 1 safety trial. *Am J Ophthalmol*. 2015;159:659–666.

37. Charbel Issa P, Kupitz EH, Heeren TFC, Holz FG. Treatment for macular telangiectasia type 2. In: Nguyen QD, Rodrigues EB, Farah ME, Mieler WF, Do DV, eds. *Developments in Ophthalmology*. Vol 55. Basel, Switzerland: Karger; 2016:189–195.

38. Koss MJ, Beger I, Koch FH. Subthreshold diode laser micropulse photocoagulation versus intravitreal injections of bevacizumab in the treatment of central serous chorioretinopathy. *Eye (Lond)*. 2012;26:307–314.

39. Wood EH, Leng T, Schachar IH, Karth PA. Multi-modal longitudinal evaluation of subthreshold laser lesions in human retina, including scanning laser ophthalmoscope-adaptive optics imaging. *Ophthalmic Surg Lasers Imaging*. 2016;47(3):268–275.

40. Kandulla J, Elsner H, Birngruber R, Brinkmann R. Noninvasive optoacoustic online retinal temperature determination during continuous-wave laser irradiation. *J Biomed Opt*. 2006;11:041111.

41. Brinkmann R, Koinzer S, Schlott K, et al. Real-time temperature determination during retinal photocoagulation on patients. *J Biomed Opt*. 2012;17:061219.

42. Seifert E, Bliedtner K, Brinkmann R. Laser speckle tracking for monitoring and analysis of retinal photocoagulation. *Proc SPIE*. 2014;89460F.